Journal of Neutron Research, Vol. 14, No. 3, September 2006, 257–268

Taylor & Francis
Taylor & Francis Group

Probing dynamics at interfaces: options for neutron and X-ray spectroscopy

MAIKEL C. RHEINSTÄDTER†*, TILO SEYDEL†, BELA FARAGO† and TIM SALDITT‡

†Institut Laue-Langevin, 6 rue Jules Horowitz, B.P. 156, 38042 Grenoble Cedex, France
‡Institut für Röntgenphysik, Friedrich-Hund Platz 1, 37077 Göttingen, Germany

(Received 23 November 2004; revised 21 September 2004; in final form 11 October 2005)

Inelastic neutron and X-ray scattering experiments on surfaces and interfaces are a challenging topic in modern physics. Particular interest arises regarding the surfaces and interfaces of soft matter and biological systems. We review both neutron and X-ray spectroscopic techniques with a view to their applicability to these samples. We discuss the different methods, namely neutron three-axis, backscattering and spin-echo spectroscopy as well as X-ray photon correlation spectroscopy (XPCS), in the context of planar lipid membrane models as an example. By a combination of the different methods, a large range in momentum and energy transfer is accessible.

Keywords: Inelastic scattering; Lipid membranes; Neutron spectroscopy; X-ray spectroscopy

1. Introduction

An outstanding problem of modern condensed matter physics relates to the question how structure, thermodynamics, phase transitions and molecular motions change from the bulk values when the spatial dimensions are reduced. In recent years, a growing interest has arisen in studying dynamics at surfaces and interfaces in as large a range of time scales as possible. While most spectroscopic techniques, such as nuclear magnetic resonance or dielectric spectroscopy, are limited to the centre of the Brillouin zone and probe the macroscopic response, neutron and X-ray scattering experiments give unique access to microscopic dynamics at length scales of, e.g. intermolecular distances. To enlarge the $\mathbf{Q}-\omega$ range to a maximum, several experimental techniques from neutron and X-ray scattering have to be combined. By combining neutron three-axis or time-of-flight, backscattering and spin-echo spectrometers, an energy range from about 50 meV (thermal three-axis or time-of-flight) down to sub-μeV (spin-echo), corresponding to timescales from about 0.1 ps to 100 ns, is accessible. X-ray photon correlation spectroscopy (XPCS) even extends this range down to the neV range and beyond (detectable motions slower than about 50 ns).

Neutron scattering gives access to length scales ranging from intermolecular distances of about 3 Å up to several hundred Å. Topics of interest are for instance the glass transition at

*Corresponding author. Email: RheinstadterM@missouri.edu

Journal of Neutron Research
ISSN 1023-8166 print/ISSN 1477-2655 online © 2006 Taylor & Francis
http://www.tandf.co.uk/journals
DOI: 10.1080/10238160600975424

the surface, the test of theoretical predictions derived from continuum mechanics, polymer surface dynamics or the dynamics of biological model systems such as planar lipid membranes. To solve these issues, several experimental challenges have to be met: the weakness of the inelastic signals necessitates a sample preparation and experimental set-up specially adapted for inelastic experiments. In this paper, we focus on the application of different inelastic scattering techniques to the study of lipid membranes as prominent examples of low dimensional systems. The understanding of dynamics in these model membranes is of fundamental interest in biophysics.

2. Lipid membranes

Phospholipid membranes are intensively studied as simple model systems to understand fundamental structural and physical aspects of their much more complex biological counterparts [1]. Dynamical properties are often less well understood in biomolecular systems, but are important for many fundamental biomaterial properties, e.g. elasticity properties and interaction forces. Lipid membrane dynamics on small molecular length scales for instance determine, or strongly affect, functional aspects like diffusion and parallel or perpendicular transport through a bilayer. Here, we discuss inelastic neutron scattering studies of the collective motions of the acyl-chains on different length and time scales. Molecular vibrations, conformational dynamics and "one particle" diffusion in the plane of the bilayer can be studied by a number of different spectroscopic techniques covering a range of different time scales such as incoherent inelastic neutron scattering or nuclear magnetic resonance or dielectric spectroscopy. In comparison, only a few experimental techniques, namely coherent inelastic neutron scattering or inelastic X-ray scattering, are able to elucidate the short range collective motions mentioned above.

Because of the weakness of the inelastically scattered signals, the preparation of appropriate samples and experimental set-ups is challenging. For the neutron three-axis, backscattering and spin-echo experiments with beam sizes of several centimeters and almost negligible absorption, solid-supported membranes were prepared. As a high purity model system the zwitterionic phospholipid dimyristoyl-phosphatidylcholine (DMPC) was chosen [2]. Figure 1(a) shows a sketch of the sample preparation. Up to 20 Si-wafers, each of them

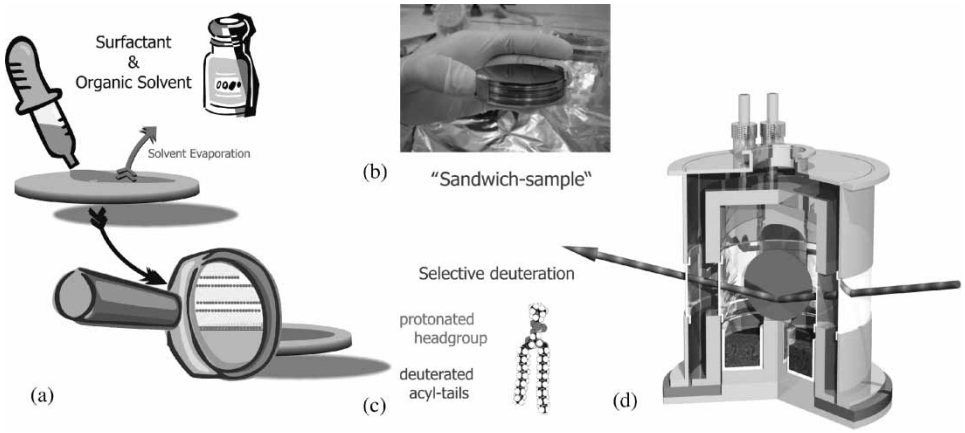

Figure 1. (a) Sketch of the sample preparation; (b) photograph of the "sandwich sample" used for the neutron experiments; (c) By selective deuteration, the collective motions of the acyl tails are enhanced over other contributions to the inelastic scattering section; and (d) Schematic of the humidity can that allows controlling temperature and humidity of the bilayers.

coated with multi-lamellar stacks of lipid bilayers and separated by small air gaps, were combined for the neutron measurements and aligned with respect to each other to create a "sandwich sample" consisting of several thousands of highly oriented lipid bilayers (total mosaicity of about 0.6°), with a total mass of up to 500 mg of deuterated DMPC, figure 1(b) shows a photograph of the sample. By selective deuteration of the acyl-chains (figure 1(c)), the respective collective motions are strongly enhanced over other contributions to the inelastic scattering cross section. The samples were kept in a closed temperature and humidity controlled aluminum chamber during the measurements (figure 1(d)). The fully hydrated, deuterated DMPC bilayers undergo a phase transition ("main transition") from the more ordered gel phase into the fluid phase at 21.5°C. Of particular interest are measurements in the physiologically relevant fluid phase.

3. Three-axis spectroscopy

The concept of three-axis spectrometry has been very successful in the investigation of collective excitations in condensed matter physics, i.e. phonons and magnons in crystals but has so far not been applied to lipid membranes. Figure 2(a) shows a schematic of a three-axis spectrometer. By varying the three axes of the instrument, the axes of rotation of the monochromator, the sample and the analyzer, the wave vectors $\mathbf{k}_i$ and $\mathbf{k}_f$ and the energies E_i and E_f of the incident and the scattered beam, respectively, can be determined. $\mathbf{Q}$, the momentum transfer to the sample and the energy transfer, ω, are then defined by the laws of momentum and energy conservation to $\mathbf{Q} = \mathbf{k}_f - \mathbf{k}_i$ and $\omega = E_i - E_f$. The accessible ($\mathbf{Q}$, ω) range of the IN12 triple axis instrument at the ILL for a fixed energy of the scattered beam E_f of 10 meV is shown in figure 2(b) and covers the $\mathbf{Q}$–ω range of the excitations in membrane systems well. It is only limited by the range of incident neutron energies offered by the neutron guide as well as by mechanical restrictions of the spectrometer. The instrumental energy resolution in this configuration is $\Delta = 500\,\mu$eV.

The combination of cold and thermal neutrons makes accessible an excitation spectrum from about 0.5 up to 50 meV. The use of highly oriented membrane stacks allowed us to perfectly align the scattering vector $\mathbf{Q}$ with respect to the lipid bilayers. $\mathbf{Q}$ can be placed in the plane of the membranes to measure static in-plane correlations, $S(\mathbf{Q}_r)$, or in-plane dynamics, $S(\mathbf{Q}_r, \omega)$. By rotating the sample by 90°, $\mathbf{Q}$ can be set perpendicular to the bilayers to probe inter-lamellar correlations to determine, e.g. the inter-lamellar spacing and the thickness of the water layer. Three-axis spectrometry thus offers the possibility of measuring

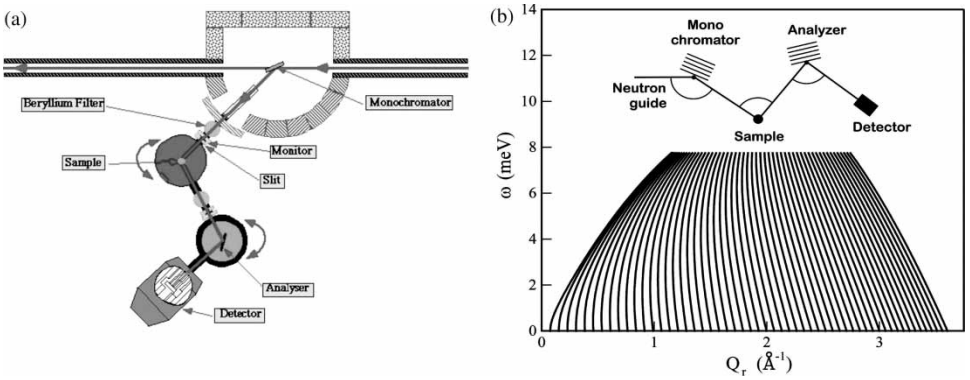

Figure 2. (a) Schematic of a three-axis spectrometer (taken from http://www.physics.uc.edu/); and (b) The accessible $\mathbf{Q}$–ω range for a typical configuration (fixed $E_f = 10$ meV) is hatched.

reflectivity, $S(\mathbf{Q}_r)$ and in-plane dynamics, $S(\mathbf{Q}_r,\omega)$, on the same instrument in the same run without changing setup [3,4]. This is an invaluable advantage since the thermodynamic state of the lipid bilayer not only depends on temperature and relative humidity, but also on cooling and heating rates, preparation and thermal history.

A typical energy scan is shown in figure 3(b). The data were collected at $T = 20°C$, in the gel phase of the bilayer at $\mathbf{Q} = 1.0\,\text{Å}^{-1}$. The inset shows the excitations of the bilayer in the gel and the fluid phase in magnification. Position and width can easily be determined from these well-pronounced peaks. Figure 3(c) shows the dispersion relation in the gel and the fluid phase as measured by several constant $\mathbf{Q}$-scans.

The particular shape of the dispersion relation resembles typical dispersions found in fluids and can qualitatively be explained. The basic scenario is the following: at small $\mathbf{Q}_r$, longitudinal sound waves in the plane of the bilayer are probed and give rise to a linear increase of $\omega \sim \mathbf{Q}_r$, saturating at some maximum value ("maxon"), before a pronounced minimum ω_0 ("roton") is observed at $\mathbf{Q}_0 \cong 1.4\,\text{Å}^{-1}$, the first maximum in the static structure factor $S(\mathbf{Q}_r)$ (the inter-chain correlation peak). Qualitatively, this can be understood if $\mathbf{Q}_0$ is interpreted as the quasi-Brillouin zone of a two-dimensional liquid (the lipid molecules arrange themselves on a two-dimensional hexagonal packed lattice). Collective modes with a wavelength of the average nearest neighbour distance $2\pi/\mathbf{Q}_0$ are energetically favourable and lead to the minimum. In perfectly ordered systems (such as crystals), the energy of the acoustic phonon branches goes down to zero at the zone centres. The static and dynamic disorder in the lipid bilayers finally leads to a minimum at finite energy values.

At $\mathbf{Q}_r$ values well above the minimum, the dispersion relation is dominated by single particle behaviour. The dispersion relation can be extracted from molecular dynamics (MD) simulations by temporal and spatial Fourier transforming the molecular real space coordinates [5] and shows excellent agreement. While the "maxon" and the high-$\mathbf{Q}$ range are

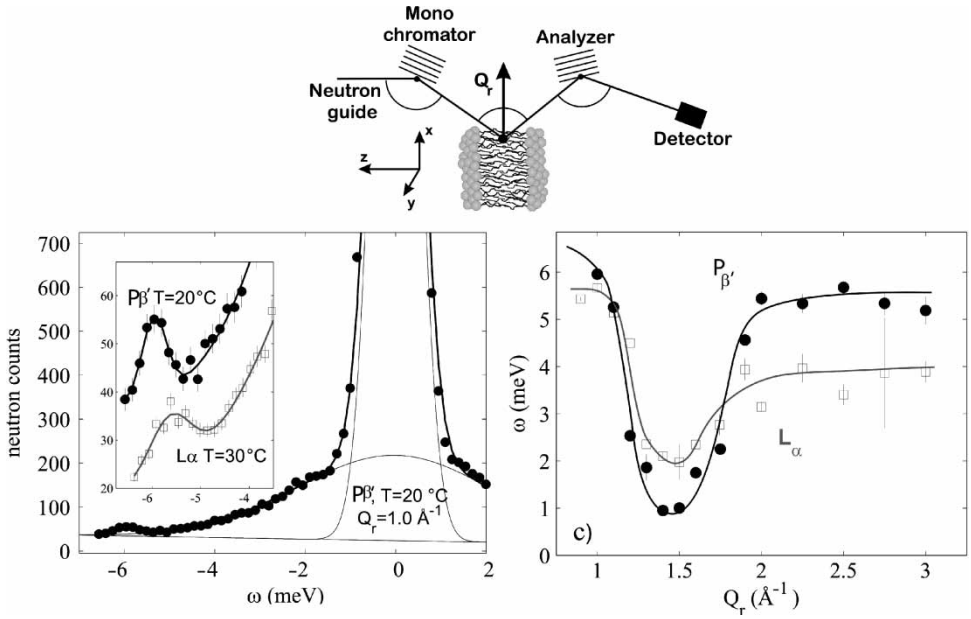

Figure 3. (a) Orientation of the bilayers with respect to the spectrometer; (b) energy scan in the gel phase of DMPC ($T = 20°C$), measured at $\mathbf{Q}_r = 1.0\,\text{Å}^{-1}$. The scattering is composed of the central elastic peak, the broad quasi-elastic background and symmetric satellites. The inset shows a zoom of the satellite peaks in both gel and fluid phase at $T = 30°C$; and (c) dispersion relations in the gel and the fluid phase of the DMPC bilayer as measured by several constant $\mathbf{Q}$ scans. (From [3]).

energetically higher in the gel than in the fluid phase due to stiffer coupling between the lipid chains in all-trans configuration, Ω_0, the energy value in the dispersion minimum, is actually smaller in the gel phase, roughly analogous to soft modes in crystals.

The range at low-**Q**-values is difficult to access by inelastic neutron scattering because of the kinetic restriction, i.e. the dispersion relation of the neutron itself. This restriction does not hold for inelastic X-ray scattering; the "dispersion" of a photon is a straight line with an extremely steep gradient.

4. Neutron backscattering spectroscopy

In backscattering experiments, the scattering function $S(\mathbf{Q},\omega)$ is directly measured analogously to three-axis spectroscopy, but contrarily to XPCS or neutron spin-echo (NSE). The high resolution obtained

$$\frac{\Delta\lambda}{\lambda} = \frac{\Delta d}{d} + \frac{\Delta\theta}{\tan\theta} \tag{1}$$

in exact backscattering is easily shown by computing the first derivative of Bragg's law (equation (1)) [6], where λ is the neutron wavelength, d the monochromator crystal lattice spacing and Θ the angle of incidence of the neutron beam with respect to the crystal surface. From this equation, it becomes clear that the monochromaticity is maximized when the angle of incidence is 90° with respect to the monochromator and analyzer crystal surface of a spectrometer. This geometry can be realized with neutrons by using adequate deflecting disk chopper devices, whereas for X-rays a perfect backscattering setup can only be approximated. For neutrons, exact backscattering was first realized at the spectrometer IN16 at the ILL [7].

Neutron backscattering spectrometers typically consist of both a backscattering monochromator and a backscattering analyzer sphere (see figure 4). The detectors are mounted very close to the sample and the discrimination between analyzed neutrons and neutrons directly scattered into the detectors is achieved by their time-of-flight. Therefore, the incident beam is pulsed by a chopper (not shown in figure 4). Taking advantage of the relatively large wavelength provided by cold neutrons, the ratio $\Delta\lambda/\lambda$ is particularly favourable and thus with the backscattering technique a Gaussian energy resolution of 0.9 μeV FHWM can routinely be achieved and a resolution of 0.45 μeV FHWM is possible at a reduced intensity.

Using the backscattering technique, two basic types of measurements can be performed: with fixed energy-window scans centred at zero energy transfer (FEW-scans), the scattered intensity arising from the sample which is elastic within the instrumental resolution can be recorded as a function of the sample temperature. From FEW-scans, information on the onset and type of molecular mobility in the sample can be inferred. The second type of measurement is the energy transfer scan. In backscattering, the energy transfer can be scanned by varying the incident energy. This is done by Doppler-shifting the incident neutron energy through an adequate movement of the monochromator crystal. Hereby, an incident neutron energy shift of about $-15\,\mu\text{eV} < \Delta E < +15\,\mu\text{eV}$ relative to the incident neutron energy can routinely be scanned, with the energy transfer limit only given by the mechanical limit of moving the monochromator crystal sufficiently fast. These energy scans correspond to a time range of motion in the sample down to a few nanoseconds. The energy transfer range can be increased to several hundred μeV by using a heatable monochromator crystal instead of a mechanically moving crystal. This setup is available at IN10 at the ILL.

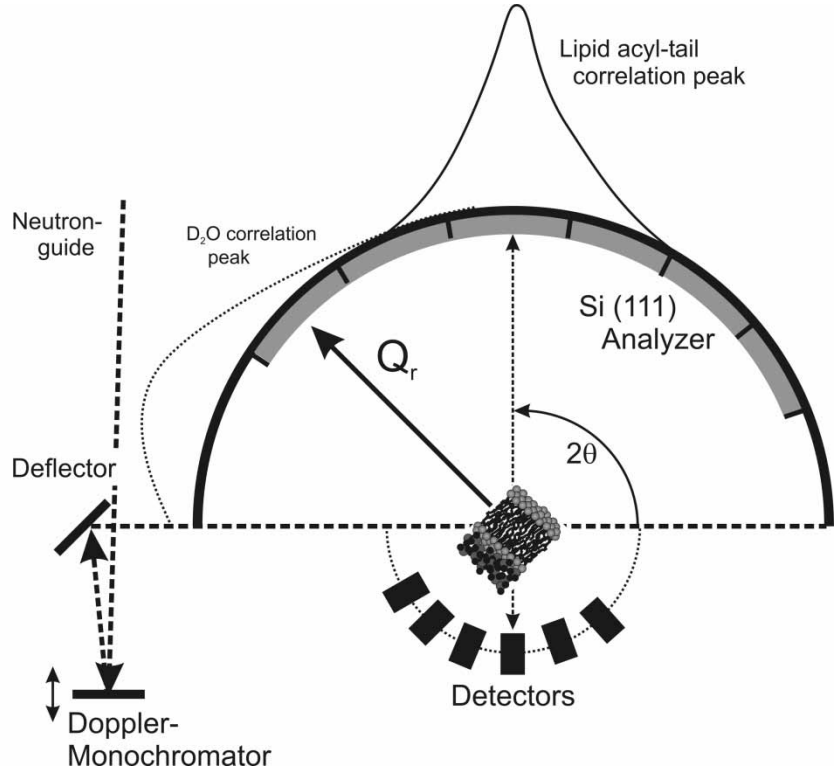

Figure 4. Schematic of the backscattering geometry at IN10. Spatially arranged analyzers allow to separately but simultaneously probe the molecular dynamics at different length scales. In our example, the inter-acyl-chain correlation peak in the plane of the membranes is located at $1.4\,\text{Å}^{-1}$ (the heavy water correlation peak would occur at $2\,\text{Å}^{-1}$).

In view at its convoluted geometry, the use of the neutron backscattering technique for probing dynamics at interfaces is challenging. Nevertheless, we have demonstrated the feasibility of backscattering on the lipid membrane sandwich samples [8]. Analogously to the three-axis experiments, we have oriented the samples in the spectrometer to measure at wave vector transfers parallel and perpendicular to the lipid membrane plane, respectively (see figure 4).

The broad lipid acyl-chain correlation peak that occurs at $\mathbf{Q}_\text{r} \cong 1.4\,\text{Å}^{-1}$ was (mainly) detected in one detector tube ("lipid detector"). A $\mathbf{Q}$-range of $0.3\,\text{Å}^{-1} < \mathbf{Q} < 1.9\,\text{Å}^{-1}$ was simultaneously detected in this set-up to investigate and discriminate molecular dynamics on the different length scales.

FEW scans were performed in a temperature range of 100–315 K to map out the transition of the lipids from immobile to mobile as a function of temperature for (a) the scattering vector $\mathbf{Q}$ placed in the plane of the membranes and (b) perpendicular to the bilayers. While the in-plane component ($\mathbf{Q}_\text{r}$) in the "lipid-detector" shows a pronounced freezing transition (figure 5(a)), there is no distinct T-dependence in the perpendicular direction ($\mathbf{Q}_\text{z}$). We interpret this in terms of correlated motions, which take place mainly in the plane of the lipid bilayers (in the time and length scales observed). We attribute the pronounced freezing step ("immobile" within the resolution window) at 294 K ($\mathbf{Q}$ centred at $1.42\,\text{Å}^{-1}$) to the main transition of the lipid acyl-chains from the rigid gel phase at low-T into the fluid phase at higher temperatures. When analysing all detectors, we find a second transition at about 271 K, mainly in the detector centred at $\mathbf{Q} = 1.85\,\text{Å}^{-1}$, which tentatively might be attributed

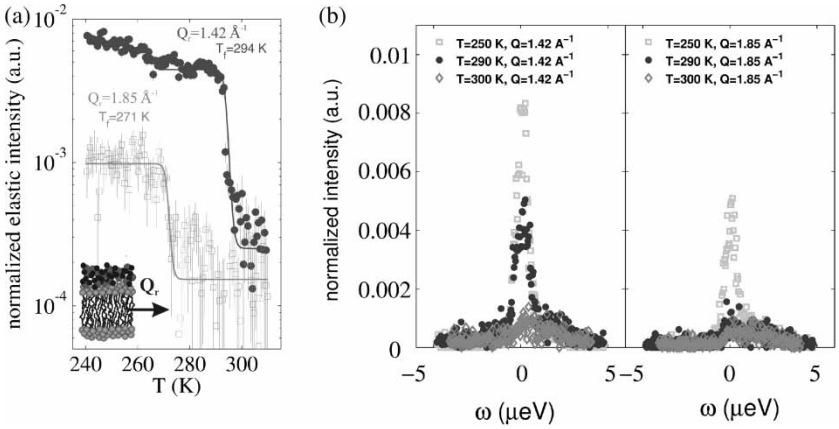

Figure 5. (a) In-plane component of the elastic scattering signal. The mobile-immobile transition (within the resolution window) is clearly different for the lipid acyl-chains ($T = 294$ K) and the position of the water correlation peak ($T = 271$ K). Solid lines are guides to the eye; and (b) energy scans at temperatures $T = 250$, 290 and 300 K for the **Q**-values 1.42 Å^{-1} (lipid acyl-chain correlation peak) and $\mathbf{Q} = 1.85\ \text{Å}^{-1}$. At 290 K, the water signal is already "mobile" within the experimental energy resolution whereas the lipid acyl-chains are still frozen. (Counting is normalized to monitor).

to the hydration water of the membrane stacks, i.e. the water layer in between the stacked membranes. Even though the detector is not perfectly centred on the maximum of the static structure factor of water at $\mathbf{Q} = 2\ \text{Å}^{-1}$ (which is not accessible on IN10), it is positioned to detect a reasonable part of the broad heavy water correlation peak. Within this interpretation, freezing of the hydration water would be lowered by about 6° as compared to (heavy) bulk water at about 277 K. Figure 5(b) displays corresponding energy transfer scans taken at three different temperatures, for $T = 250$, 290 and 300 K with a typical counting time of about 9 h per temperature. An elastic peak in the inelastic spectra points to static order at the corresponding length scales, where a fluid system has no order at infinitely long time scales. Even within the very limited statistics, the different dynamics is clearly visible: while the lipid acyl-chains melt between 290 and 300 K, melting at the water position already occurs between 250 and 290 K.

Our experiment gives a first high energy-resolution wave vector-resolved insight into collective lipid membrane dynamics. The dynamical properties of hydration water may be different from those of bulk water because hydrogen bonding to the lipid head groups at the lipid–water interface of the membrane might slow down water rotation and translation. A scenario with gradual freezing of the water molecules, depending on the distance to the water–lipid interface, is also under discussion.

Further measurements and data analysis are in progress and with this technique the melting temperatures of the lipid layers and the membrane water will be mapped out. In addition, further experiments will focus on whether the melting is accompanied by a quasi-elastic broadening. This would be an indication of whether or not phase or glass transitions are present in this system.

5. Neutron spin-echo spectroscopy

NSE is a clever way of reaching very high energy resolution with neutrons close to 10^{-5} of the incoming neutron energy without sacrificing intensity [9]. With the latest development in instrumentation [10,11], the gap between photon correlation spectroscopy (X-ray and visible light) is getting smaller and smaller. Offering the possibility to cover the dynamics in systems

over 5–7 decades in space (**Q** range) as well as in energy (time space) unavoidably leads us to a more complete description of the physical systems.

With NSE the directly measured quantity is $S(\mathbf{Q}, t)/S(\mathbf{Q}, 0)$, that is we measure directly the time dependence. Here

$$t \propto \lambda^3 \int B \, \mathrm{d}l \tag{2}$$

B is the magnetic field of the precession coils and the integral is taken over the coil length. Usually the magnetic field is varied to cover the time range we are interested in. It is important to note the strong dependence of the time parameter with the wavelength. Essentially the limiting factor for the maximum reachable Fourier time is due to the residual field inhomogeneities [12], nevertheless choosing longer wavelengths still extends the time range. Long wavelength has a second benefit for surface studies. In reflection, the angles we are dealing with become bigger for a given **Q** value, thus the sample size to cover the usually large neutron beam (usually in the cm range) is smaller. Presently, there exists no dedicated NSE spectrometer for reflectivity studies. The experiment we will describe in the following [14] was performed on the IN15 NSE spectrometer at the ILL. The sample was a smectic liquid crystal 4-octyl-40-cyanobiphenyl (8CB) with the C8H17 chain deuterated to enhance the neutron contrast.

The repeat distance of the smectic layers leads to a sharp diffraction peak at $\mathbf{Q}_z = 0.18\,\text{Å}^{-1}$. With 9.4 Å incoming neutron wavelengths this corresponds to 16.8° scattering angle. The film dynamics is expected to be seen only if **Q** has a component parallel to the film ($q_\perp$). As the NSE spectrometer uses a not too tightly monochromatic beam ($\Delta\lambda/\lambda = 11\%$ FWHM) but a relatively tight angular collimation (about 0.5°), the most convenient way to move off the Bragg peak is to rotate the sample. With the 16.8° scattering angle, we could easily rotate the sample ±5° without obscuring the incoming or outgoing beams. On figure 6, the scattering geometry is represented with the sample turned horizontal for better visibility [13].

IN15 has a 2D detector, thus the in-plane $q_\perp$ component can be calculated as follows:

$$q_\perp = \frac{2\pi}{\lambda}\sqrt{\left(\cos(\Delta\varphi)\cos\left(\frac{\vartheta_0}{2} + \Delta\psi - \omega\right) - \cos\left(\frac{\vartheta_0}{2} + \omega\right)\right)^2 + (\sin(\Delta\varphi))^2}, \tag{3}$$

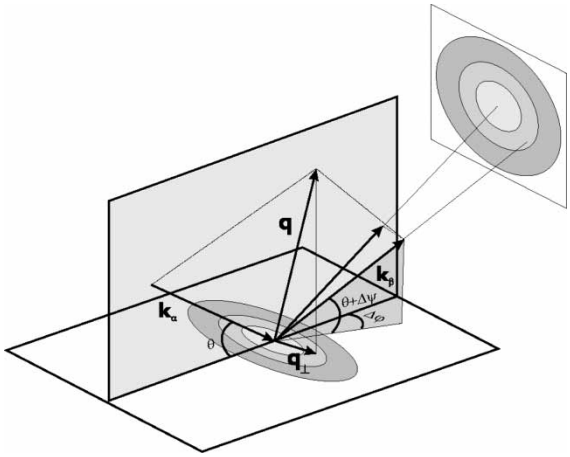

Figure 6. Sketch of the spin-echo scattering geometry.

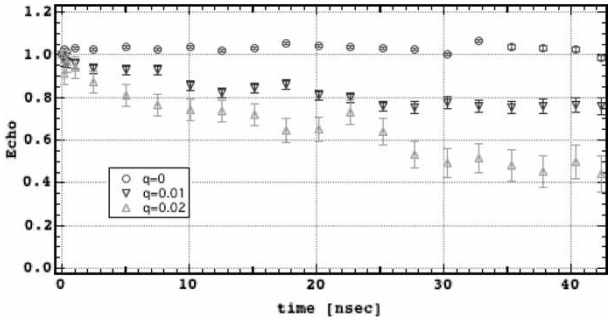

Figure 7. NSE decay curves for different $q_\perp$-values.

where ϑ_0 is the scattering angle, ω is the sample rotation and $\Delta\psi, \Delta\varphi$ are angles which correspond to the pixel positions on the 2D detector relative to the centre. Typical NSE decay curves are shown in figure 7. The $q_\perp = 0$ curve corresponds to the Bragg peak and within the instrument resolution it is elastic. All the other curves could be well described with a stretched exponential with $\beta = 0.6$ exponent. Taking into account the bending elasticity of the film [13,19], NSE measurements extend the **Q** range to a new regime of previous XPCS results with good agreement with theory (figure 8). Surely, new experiments will follow in the fast expanding field of surfaces and interfaces.

Maybe some words should be said on possible pitfalls concerning NSE experiments. In fact, some kind of elastic scatterer is always measured to calibrate the instrument resolution. As we measure $S(\mathbf{Q}, t)$ directly, the deconvolution of the instrumental resolution in ω-space, becomes a simple division. Different neutron trajectories explore slightly different field integrals, thus leading to finite instrumental resolution. Special care has to be taken that the elastic scatterer mimics as closely as possible the scattering profile and geometry of the real sample. Indeed, the unusually long sample and thin slits introduce very specific correlations between positions and trajectories, which can give artefacts which sometimes very much look like real effects.

A closer look on the NSE curves shown above reveals that the Bragg peak, while very close to 1.0, is not quite within the error bars. After different trials, for the resolution measurement we used a strongly scattering grafoil piece placed exactly where the film was, in the same sample holder with the same slits. The only difference which remained, was that the sharp Bragg peak from the sample actually remonochromates the beam better than the

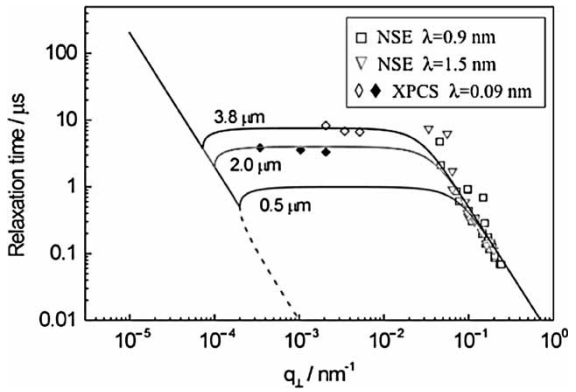

Figure 8. Experimental relaxation times for samples of 8CB. Squares: NSE at wavelength of 0.9 nm; triangles: NSE at 1.5 nm; diamonds: XPCS at 0.09 nm for two membrane thicknesses; and solid line: calculated dispersion curves [14].

original 15% monochromatization. Such effects are particularly dangerous on the side of strong peaks. In our case when the sample was rotated at least 1°, the Bragg peak moved off the 2D detector and the scattered intensity was more uniform. + and − rotation gave also identical results, thus we are rather confident that artefacts are at most, somewhat smaller than the deviation of the NSE curve from 1.0 on the Bragg peak.

6. X-ray photon correlation spectroscopy

For only a few years, it has become possible to study lateral dynamics at surfaces in the most direct and unambiguous way using XPCS [15,16,17,20]. XPCS requires (partially) coherent X-rays which are only available at the most advanced synchrotron sources. The basic idea of XPCS is to record the intensity autocorrelation of the speckles visible in coherently illuminated matter. This can be done with an excellent wave vector resolution. In measuring the intensity correlation in time, XPCS somewhat resembles the neutron spin-echo technique in that the intermediate scattering function $S(\mathbf{Q}, t)$ rather than $S(\mathbf{Q}, \omega)$ is accessed. Surface XPCS takes advantage of the critical angle for total external reflection for X-rays impinging through vacuum or air onto a surface which is greater than zero (see figure 9). Therefore, it is

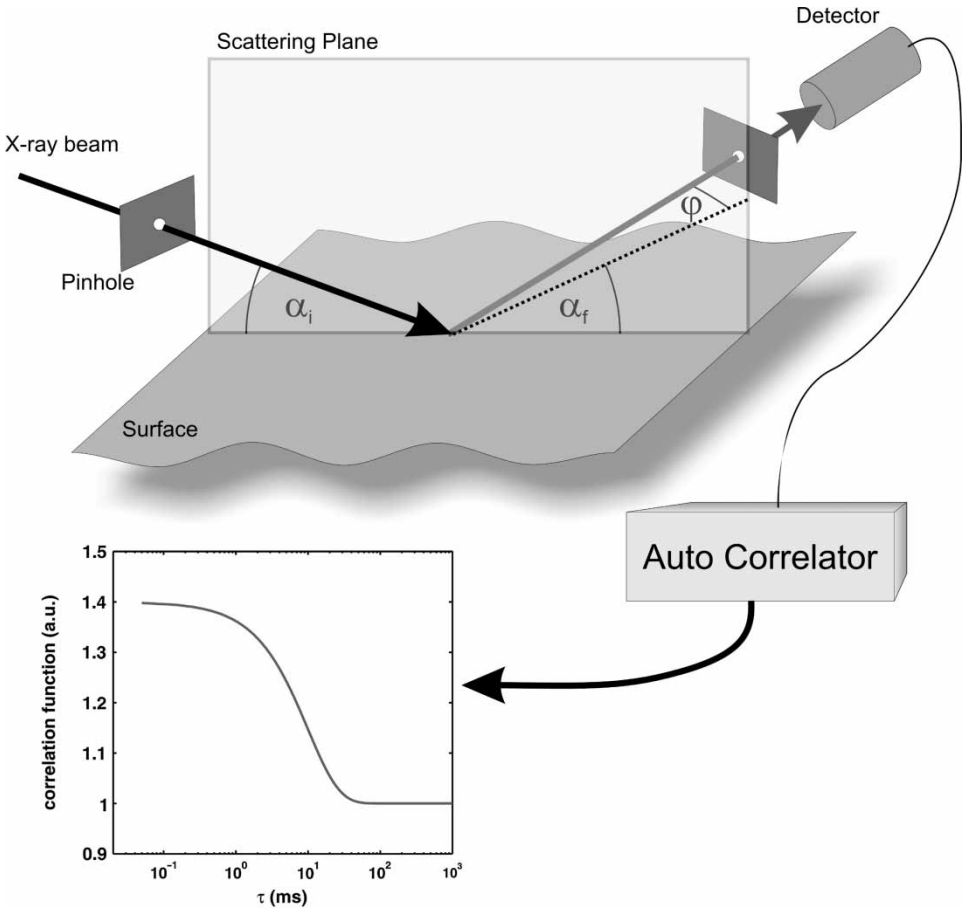

Figure 9. Schematic of the XPCS set-up for surface scattering and sketched theoretical curve of a single exponential decay as expected in the intensity autocorrelation from a simple relaxational motion.

possible to illuminate surfaces under grazing angles of incidence and to detect a scattering pattern arising from the near-surface region restricted by the $1/e$-penetration depth of the evanescent X-ray wave field.

Surface XPCS has the additional advantage that the available coherence volume is projected onto the surface under grazing angles. Therefore, several hundred micrometers can be coherently illuminated along a surface, even though the typical transverse coherence length at 8 keV at 3rd generation light sources is only of the order of 10 μm. In addition to being surface sensitive, XPCS has the advantage over visible laser light scattering that shorter length scales may be probed and opaque materials may be studied. However, so far the promise of reaching shorter length scales has been severely limited by the photon count rate. Even at the most brilliant sources available today the maximum attainable wave vector transfer is restricted by the limited coherent flux. In addition, there is a fundamental limit regarding the shortest attainable time scales using XPCS. This limit is caused by the intrinsic time structure of the electron bunches within any synchrotron storage ring and is of the order of a few nanoseconds. Furthermore, because the inelastic or quasi-elastic processes in the sample are recorded through the intensity autocorrelation function, the minimum intensity that is required to obtain meaningful data is essentially proportional to the frequency to be detected in the sample.

Recently, some of the present authors have performed a first experiment using coherent X-ray radiation at the Troïka 1 beam line of the ESRF to study solid-supported lipid membranes (DMPC) as well as charged surfactant bilayers [18,19]. The original idea was to probe collective membrane dynamics on mesoscopic length scales, such as undulation modes. Note that much work in the literature has been dedicated to the analysis of elastic X-ray scattering in terms of thermal diffuse scattering, without being able to directly evidence the corresponding relaxation time scales. In contrast to the expected smooth scattering curve, averaged out by the fluctuations, we have recorded a pronounced (static) speckle pattern in the diffuse scattering when measuring with coherent X-ray beams. Static speckles were observed at small to medium parallel momentum transfer accessible by scans in the plane of incidence (rocking scan, detector scans), at positions corresponding to the diffuse Bragg sheet where the multi-lamellar stack dominates the signal.

On the other hand, the curves recorded over a range of higher parallel momentum transfer out of the plane of incidence were smooth. This finding might be explained if we assume that in the small **Q** regime, the diffuse signal stems predominantly from static defects and domain scattering, while at high-**Q**, the signal of truly dynamic thermal disorder prevails, which would average out the speckle pattern in time to a continuous curve. However, other effects, such as substrate interactions and geometrical effects [20] may also have to be taken into account. At the same time, we were not able to record an XPCS signal in the high-**Q** range, possibly because the dynamics were too fast and the photon count rate too small. This conclusion is supported by numerical estimations based on smectic hydrodynamics, which predicts a strong increase of the frequency at high-**Q**. Contrarily, free-standing films also exhibit much slower acoustic modes, which correspond to centre of mass movement of the whole film [14]. In smectic films or multi-lamellar membranes deposited on solid surfaces, the low-**Q** acoustic modes are suppressed by the boundary conditions of the flat substrate.

The present work points out a caveat for the X-ray line shape analysis of smectic systems from which the membrane elasticity is deduced. Contrarily, inelastic neutron experiments do not suffer from this limitation, since they probe the inelastically scattered neutrons directly and therefore separate out the elastic scattering. In view of these limits in time scale and competing elastic scattering, it is clearly worth further developing of neutron-based instruments and methods to apply inelastic and quasi-elastic neutron scattering to surfaces and interfaces. To this end, collective undulations and bending motions of lipid membranes probed by spin-echo (see previous section) present an encouraging example.

7. Conclusion

In summary, we have illustrated the potential relevance of inelastic scattering techniques to study dynamics of surfaces and interfaces, taking the example of planar lipid membranes. The combination of the different technique-neutron three-axis, backscattering and spin-echo spectroscopy, as well as XPCS-maximizes the accessible $\mathbf{Q}-\omega$ range covering nine decades in energy transfer and spatial dimensions from intermolecular distances to several hundred μm. The dynamics in biomimetic membranes is of particular interest in membrane biophysics to better understand the highly complex dynamics of biological membranes. An understanding of membrane dynamics can also be useful to tailor membrane properties for biotechnology applications.

Acknowledgements

We thank Christoph Ollinger (Institut für Röntgenphysik, Göttingen) for help in sample preparation and for an enjoyable collaboration in some of the original studies, Giovanna Fragneto (ILL) for support and collaboration on related studies, Matthias Elender (ILL) for technical and engineering support and the ILL and the ESRF for allocation of beam time.

References

[1] R. Lipowsky and E. Sackmann, Structure and dynamics of membranes. *Handbook of Biological Physics* (Elsevier, North-Holland, Amsterdam, 1995), Vol. 1.
[2] C.M. Münster, T. Salditt, M. Vogel, R. Siebrecht and J. Peisl, Europhys. Lett. **46** 486 (1999).
[3] M.C. Rheinstädter, C. Ollinger, G. Fragneto, F. Demmel and T. Salditt, Phys. Rev. Lett **93** 108107 (2004).
[4] M.C. Rheinstädter, C. Ollinger, G. Fragneto and T. Salditt, Physica B **350** 136 (2004).
[5] M. Tarek, D.J. Tobias, S.-H. Chen and M.L. Klein, Phys. Rev. Lett. **87** 238101 (2001).
[6] H. Maier-Leibnitz, Nukleonik **8** 61 (1966).
[7] B. Frick and M. Gonzalez, Physica B **301** 8 (2001).
[8] M.C. Rheinstädter, T. Seydel, F. Demmel and T. Salditt, Phys. Rev. E **71** 061908 (2005).
[9] F. Mezei, The principles of neutron spin echo. in *Neutron Spin Echo,* Lecture Notes in Physics, edited by F. Mezei (Springer Verlag, Berlin, 1980), Vol. 128, pp. 3–26.
[10] B. Farago, Physica B **268** 270 (1999).
[11] P. Schleger, G. Ehlers, A. Kollmar, B. Alefeld, J.F. Barthelemy, H. Casalta, B. Farago, P. Giraud, C. Hayes, C. Lartigue, F. Mezei and D. Richter, Physica B **266**(1–2) 49 (1999).
[12] F. Mezei, C. Pappas, and T. Gutberlet (Editors), Neutron spin echo spectroscopy. *Lecture Notes in Physics* (Springer Verlag, Berlin, 2003), Vol. 601.
[13] I. Sikharulidze and W.H. de Jeu, Phys. Rev. E **72** 011704 (2005).
[14] I. Sikharulidze, B. Farago, I.P. Dolbyna, A. Madsen and W.H. de Jeu, Phys. Rev. Lett. **91** 165504 (2003).
[15] T. Seydel, A. Madsen, M. Tolan, G. Grübel and W. Press, Phys. Rev. B **63** 073409 (2001).
[16] T. Seydel, A. Madsen, M. Sprung, M. Tolan, G. Grübel and W. Press, Rev. Sci. Instrum. **74** 4033 (2003).
[17] A. Madsen, T. Seydel, M. Sprung, C. Gutt, M. Tolan and G. Grübel, Phys. Rev. Lett. **92** 096104 (2004).
[18] G. Brotons, D. Constantin, A. Madsen and T. Salditt, Physica B **357** 28 (2005).
[19] T. Salditt, D. Constantin, G. Brotons and A. Madsen (In press).
[20] A. Madsen, T. Seydel, M. Tolan and G. Grübel, J. Synchroton Radiation **12** 786 (2005).